Spin Pumping with Coherent Elastic Waves

M. Weiler,[1] H. Huebl,[1] F. S. Goerg,[1] F. D. Czeschka,[1] R. Gross,[1,2] and S. T. B. Goennenwein[1,*]

[1]*Walther-Meißner-Institut, Bayerische Akademie der Wissenschaften, 85748 Garching, Germany*

[2]*Physik-Department, Technische Universität München, 85748 Garching, Germany*

(Received 6 October 2011; published 23 April 2012)

We show that the resonant coupling of phonons and magnons can be exploited to generate spin currents at room temperature. Surface acoustic wave pulses with a frequency of 1.55 GHz and duration of 300 ns provide coherent elastic waves in a ferromagnetic thin-film–normal-metal (Co/Pt) bilayer. We use the inverse spin Hall voltage in the Pt as a measure for the spin current and record its evolution as a function of time and external magnetic field magnitude and orientation. Our experiments show that a spin current is generated in the exclusive presence of a resonant elastic excitation. This establishes acoustic spin pumping as a resonant analogue to the spin Seebeck effect.

DOI: 10.1103/PhysRevLett.108.176601 PACS numbers: 72.25.Mk, 75.78.−n, 75.80.+q, 76.50.+g

The generation and detection of pure spin currents is vigorously investigated for the injection and transportation of spin information [1–6]. Spin currents may be generated, e.g., via the spin Seebeck effect [7–10] or via spin pumping [6,11–16]. In the latter approach, electromagnetic waves in the GHz regime, i.e., microwave *photons*, are used to resonantly excite magnetization dynamics in a ferromagnet and thus drive a spin current into an adjacent normal metal. Here, we show that the resonant absorption of elastic waves, i.e., microwave *phonons*, in a ferromagnet–normal-metal bilayer can be used to acoustically drive a spin current. This establishes the spin-current generation by a resonant phonon-magnon coupling and thus an interaction of lattice and spin degrees of freedom. In this sense, acoustic spin pumping can be seen as a resonant analogue of the spin Seebeck effect [17]. This resonant magnon-phonon coupling is a complementary approach to the nonresonant acoustic spin-current generation recently observed by Uchida *et al.* [18] in a ferromagnetic insulator. In particular, we use a metallic ferromagnet and are able to tune the system in and out of acoustically driven ferromagnetic resonance via the application of an external magnetic field. As shown in the following, we find clear evidence for a resonant spin-current generation. However, within the experimental sensitivity limit, we do not observe a spin current in the off-resonant condition. Our findings are thus in accordance with conventional, photon-ferromagnetic-resonance (FMR)-driven, spin pumping experiments. The resonant phonon-spin-current conversion discussed in this Letter opens intriguing perspectives for applications in, e.g., microelectromechanical systems, since elastic deformation can now be used for spin-current generation. Thus, phonon-driven spin pumping is a pathway for the resonant generation of a spin current in the absence of a real, external electromagnetic driving field. Furthermore, phonon-driven spin pumping can be disentangled from microwave rectification effects induced by free space electromagnetic waves [19–21]. Using time-resolved experiments, we are able to clearly distinguish such rectification effects from the inverse spin Hall voltage [22,23] used to detect the acoustically driven spin pumping.

To demonstrate spin pumping via microwave phonons, we exploit phonon-driven FMR [24] in ferromagnet–normal-metal bilayers. The acoustic FMR is excited by a surface acoustic wave (SAW) propagating in a cobalt-platinum (Co/Pt) thin-film bilayer in the presence of an externally applied, static magnetic field. Via inverse magnetostriction [25], the SAW induces magnetization dynamics in the Co thin film which in turn generate a spin current at the Co/Pt interface. The sample is depicted schematically in Fig. 1(a). It consists of a Co(10 nm)/Pt(7 nm) bilayer deposited on $LiNbO_3$ between two Al (70 nm) interdigital transducers (IDTs) [26] with a periodicity of 20 μm. For all results shown in this Letter, the acoustic delay line shown in Fig. 1(a) is operated at its 9th harmonic frequency $\nu = 1.548$ GHz at room temperature. A SAW is launched at the input IDT and induces a time varying pure lattice strain $\varepsilon(t) = \varepsilon \cos(2\pi\nu t)$ along $\boldsymbol{x}$ with amplitude ε into the ferromagnet [27]. Via magnetoelastic coupling, $\varepsilon(t)$ excites magnetization $\boldsymbol{M}$ precession as depicted schematically in Fig. 1(b). The magnetization precession can relax via the emission of a spin current $\boldsymbol{J}_s$ into the normal metal (Pt) [12]. We detect $\boldsymbol{J}_s$ along $\boldsymbol{z}$ via the inverse spin Hall effect [22], which results in an electric field $\boldsymbol{E}_{\mathrm{ISH}} \propto \boldsymbol{M} \times \boldsymbol{J}_s$. More precisely, we measure $V_{\mathrm{DC}} \propto \boldsymbol{E}_{\mathrm{ISH}} \cdot \boldsymbol{y}$ [cf. Fig. 1(b)]. The input IDT generates not only a SAW but also an electromagnetic wave (EMW) upon the application of a rf voltage. Thus, the aforementioned microwave rectification effects can contribute significantly to V_{DC}. However, since the velocity of the SAW (the speed of sound) is about 5 orders of magnitude slower than that of the EMW (the speed of light), a time-resolved study of V_{DC} and the transmitted SAW power P_{IDT} allows for a separation of SAW- and EMW-driven effects. We thus apply SAW pulses as depicted in Fig. 1(c) and study the time-dependent evolution of V_{DC} and P_{IDT} using a two-channel

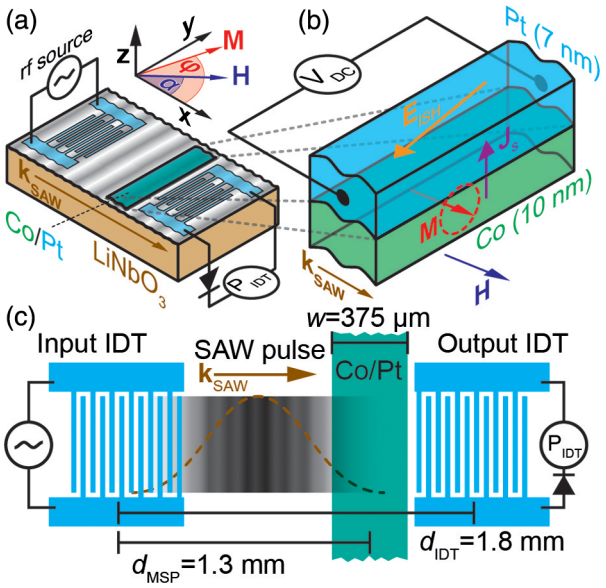

FIG. 1 (color online). (a) Schematic view of a $LiNbO_3$/Co/Pt hybrid. An external static magnetic field $\boldsymbol{H}$ can be applied within the film plane at an angle α to the SAW propagation direction. (b) The SAW drives resonant magnetization $\boldsymbol{M}$ precession that emits a spin current $\boldsymbol{J}_s$ into the Pt. $\boldsymbol{J}_s$ is detected via the inverse spin Hall effect in the Pt thin film, i.e., as the voltage V_{DC}. (c) Sample geometry (not to scale). The SAW pulse first traverses the Co/Pt bilayer and then is detected at the output IDT.

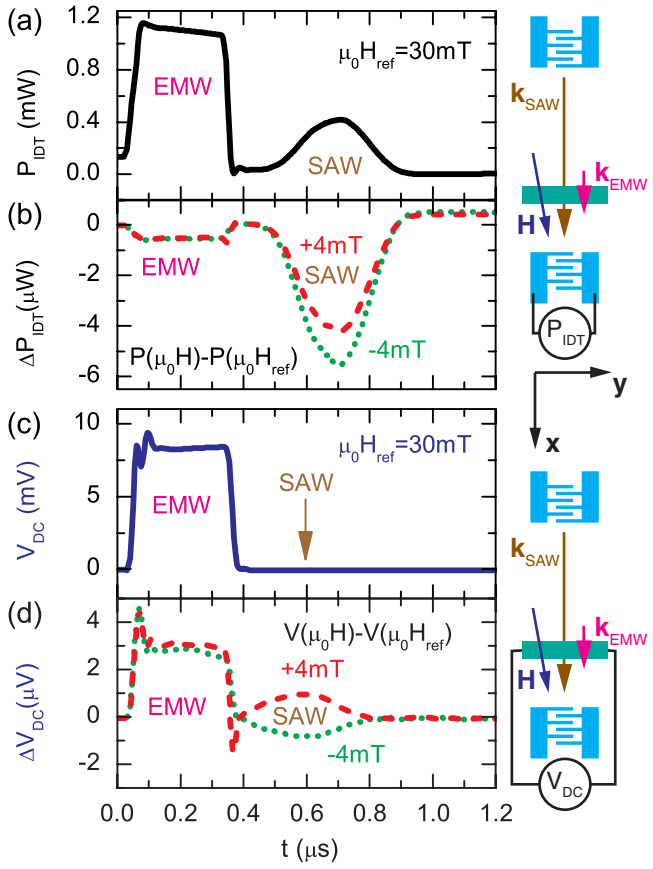

FIG. 2 (color online). Time-resolved spectroscopy with $\boldsymbol{H}$ applied at $\alpha = 10°$. (a) P_{IDT} as a function of time with $\mu_0 H_{\mathrm{ref}} = 30$ mT, showing the detection of the EMW (0.2 μs) and the SAW (0.7 μs) pulses at the output IDT. (b) $\Delta P_{\mathrm{IDT}}(t) = P_{\mathrm{IDT}}(t, \mu_0 H) - P_{\mathrm{IDT}}(t, \mu_0 H_{\mathrm{ref}})$. $\Delta P_{\mathrm{IDT}}(0.7\ \mu\mathrm{s}) < 0$ shows that the SAW is damped for $\mu_0 H_{\mathrm{res}} = \pm 4$ mT, indicating acoustically driven FMR. (c) V_{DC} as a function of time at $\mu_0 H_{\mathrm{ref}} = 30$ mT. The EMW is rectified at the bilayer. (d) $\Delta V_{\mathrm{DC}}(t) = V_{\mathrm{DC}}(t, \mu_0 H) - V_{\mathrm{DC}}(t, \mu_0 H_{\mathrm{ref}})$. The change of sign of $\Delta V_{\mathrm{DC}}(0.6\ \mu\mathrm{s})$ with the reversal of the $\boldsymbol{H}$ direction is a signature of acoustic spin pumping.

oscilloscope. For the generation of the SAW pulses, we apply +30 dBm rf pulses with $\nu = 1.548$ GHz, a pulse width $t_w = 310$ ns, and a pulse period $t_r = 57.3$ μs to the input IDT. By studying $P_{\mathrm{IDT}}(t)$ and $V_{\mathrm{DC}}(t)$ for various external magnetic field $\boldsymbol{H}$ orientations and magnitudes, we can unambiguously identify phonon-driven spin pumping, as shown in the following.

We first turn to the separation of contributions to P_{IDT} and V_{DC} due to the SAW and the EMW. In Fig. 2(a), we show the transmitted rf power P_{IDT} as a function of time t for application of $\boldsymbol{H}$ at $\alpha = 10°$. As the SAW has a velocity of 3440 m/s and the sample features a center-to-center IDT spacing of 1.8 mm, the SAW transit time is $t_t = 0.52$ μs . In contrast, the EMW propagates with the speed of light and is thus expected to appear almost instantaneously with the microwave pulse at $t \approx 0$. Indeed, in the $P_{\mathrm{IDT}}(t)$ trace shown in Fig. 2(a), two signals are observed, the first of which begins at $t \approx 0$ and is attributed to the EMW. The rectangular shape and duration mimic the applied microwave pulse. At $t_{\mathrm{SAW}} = 0.7$ μs, a Gaussian pulse of smaller magnitude is recorded. This pulse is due to the SAW reaching the output transducer. The separation of EMW and SAW pulses allows us to distinguish between photon- and phonon-driven contributions to $P_{\mathrm{IDT}}(t)$. We now turn to the external magnetic field dependence of P_{IDT}, shown in Fig. 2(b). Here, we plot $\Delta P_{\mathrm{IDT}} = P_{\mathrm{IDT}}(\mu_0 H) - P_{\mathrm{IDT}}(\mu_0 H_{\mathrm{ref}})$. We use $\mu_0 H_{\mathrm{ref}} = 30$ mT as a reference magnetic field and investigate data obtained at the FMR magnetic field $\mu_0 H_{\mathrm{res}} = \pm 4$ mT (dashed and dotted lines, respectively). For both values of H, one observes a pronounced dip in ΔP_{IDT} at t_{SAW}. This SAW attenuation is attributed to acoustically driven FMR, which results in a damping of the SAW, as detailed in Ref. [24]. We now turn to the simultaneously recorded voltage $V_{\mathrm{DC}}(t)$ in the Co/Pt bilayer. Since the latter is positioned at a distance of $d_{\mathrm{MSP}} = 1.3$ mm from the input IDT, the SAW pulse is expected to reach the bilayer 0.1 μs before it is detected at the output IDT. This yields a maximum SAW amplitude at the bilayer at $t_{\mathrm{MSP}} = 0.6$ μs, while the EMW is again expected at $t \approx 0$. For $\mu_0 H_{\mathrm{ref}} = 30$ mT, we observe $V_{\mathrm{DC}}(t)$, shown in Fig. 2(c), dominated by EMW-driven effects, as is evident from its time dependence and shape. In particular, no signal is observed at t_{MSP}. This is not surprising, since no acoustic FMR and thus no spin

current are excited for these parameters. In contrast, the FMR condition is fulfilled at $\mu_0 H_{\mathrm{res}} = \pm 4$ mT. In Fig. 2(d), we plot $\Delta V_{\mathrm{DC}} = V_{\mathrm{DC}}(\mu_0 H) - V_{\mathrm{DC}}(\mu_0 H_{\mathrm{ref}})$ for $\mu_0 H = \pm 4$ mT (dashed and dotted lines, respectively). Here, a clear feature can be observed at t_{MSP}. The sign reversal of $\Delta V_{\mathrm{DC}}(t_{\mathrm{MSP}})$ with respect to the $\boldsymbol{H}$ direction thereby is a necessary condition for the detection of a spin current via the inverse spin Hall effect [15]. In contrast, the EMW causes a field-symmetric contribution to ΔV_{DC}, which means that no EMW-driven spin pumping is observed.

The contributions to ΔP_{IDT} and ΔV_{DC} due to the SAW and EMW are now investigated as a function of H. We hereby take advantage of the separation of the SAW and EMW in the time domain and attribute $\Delta P_{\mathrm{IDT}}(0.2\ \mu\mathrm{s})$ and $\Delta V_{\mathrm{DC}}(0.2\ \mu\mathrm{s})$ to the interaction of the bilayer with the EMW and $\Delta P_{\mathrm{IDT}}(0.7\ \mu\mathrm{s})$ and $\Delta V_{\mathrm{DC}}(0.6\ \mu\mathrm{s})$ to the interaction of the SAW and the bilayer. Figure 3(a) shows $\Delta P_{\mathrm{IDT}}(\mu_0 H)$ for both elastic and electromagnetic interactions. We find a very weak magnetic field dependence of the transmission of the EMW (solid symbols) which shows no indication for FMR driven by the EMW. We do, however, observe a distinct resonant absorption of the SAW (open symbols), which we attribute to acoustically driven FMR [24]. Turning to ΔV_{DC}, shown in Fig. 3(b), we in contrast observe a sizeable magnetic field dependence of the EMW transmission at $t = 0.2\ \mu$s (solid symbols) attributed to microwave rectification effects [20]. The signal shape, however, is distinctly different from that expected for the spin pumping effect; in particular, no reversal of the sign of ΔV_{DC} with reversal of the $\boldsymbol{H}$ direction is observed.

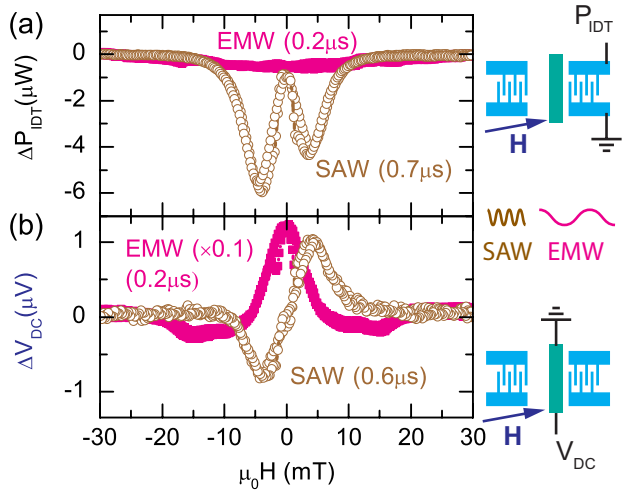

FIG. 3 (color online). (a) ΔP_{IDT} for the detection of the SAW (open symbols) and the EMW (solid symbols) pulses at the output IDT as a function of external magnetic field magnitude for $\boldsymbol{H}$ applied at $\alpha = 10°$. (b) ΔV_{DC} for the detection of the SAW (open symbols) and the EMW (solid symbols) pulses at the bilayer. The characteristic fingerprint for acoustic spin pumping is the antisymmetric behavior of ΔV_{DC} with respect to the $\boldsymbol{H}$ orientation.

A detailed investigation of the origin and evolution of ΔV_{DC} due to EMW rectification is beyond the scope of this Letter. We refer to Refs. [28,29]. At $t_{\mathrm{MSP}} = 0.6\ \mu$s (open symbols), however, only the SAW pulse is present. Here, ΔV_{DC} shows a magnetic field dependence characteristic for spin pumping, in particular, featuring a sign reversal with reversal of the $\boldsymbol{H}$ direction and extrema at the FMR H field. We furthermore checked whether rf currents induced by the SAW E field into the Co/Pt could cause $\Delta V_{\mathrm{DC}}(0.6\ \mu\mathrm{s})$. To this end, we deliberately applied such rf currents with $\nu = 1.548$ GHz to the bilayer [30], which resulted in a dc photovoltage V_{pv} attributed to rectification effects [28,29,31] and spin-torque FMR [32]. As detailed in the Supplemental Material [30], the magnetic field dependence of V_{pv} is distinctly different to that of $\Delta V_{\mathrm{DC}}(0.6\ \mu\mathrm{s})$. We thus attribute $\Delta V_{\mathrm{DC}}(0.6\ \mu\mathrm{s})$ solely to elastically driven spin pumping.

To show the crucial separation of EMW- and SAW-driven contributions [$\Delta V_{\mathrm{DC}}(\mathrm{EMW}) \gg \Delta V_{\mathrm{DC}}(\mathrm{SAW})$] in a more complete fashion, we plot ΔP_{IDT} and ΔV_{DC} as a function of t and $\mu_0 H$ in Figs. 4(a) and 4(b), respectively (only the magnetic field upsweep is shown). EMW rectification is observed for $t < 0.375\ \mu$s, yielding a field-symmetric contribution to ΔV_{DC}. For the times corresponding to the presence of the SAW pulse, both ΔP_{IDT} and ΔV_{DC} are finite only for a narrow range around the FMR magnetic field $\mu_0 H_{\mathrm{res}} = \pm 4$ mT. One can observe that ΔP_{IDT} is retarded by about 0.1 μs with respect to ΔV_{DC} (indicated by the dashed lines), in accordance to the propagation of the SAW along the delay line. For the investigation of phonon-driven spin pumping with a good signal-to-noise ratio, we average ΔP_{IDT} and ΔV_{DC} for the time range indicated by the dashed lines. This yields the phonon-driven ΔP_{SAW} and the magnetoelastic spin pumping (MSP) voltage ΔV_{MSP}, respectively. ΔP_{SAW} and ΔV_{MSP} are plotted in Fig. 4(c) as a function of H (solid symbols: H upsweep; open symbols: H downsweep). While a field-symmetric absorption of rf power is observed for ΔP_{SAW}, as expected for acoustically driven FMR [24], ΔV_{MSP} shows the antisymmetric behavior with respect to the $\boldsymbol{H}$ orientation reversal characteristic of spin pumping. Furthermore, the resonance field and linewidth of ΔP_{SAW} and ΔV_{MSP} coincide. Outside of acoustically driven FMR (i.e., $\mu_0 |H| > 10$ mT), the SAW and thus phonons are still present in the ferromagnetic thin film. However, within the resolution of our experiment, $\Delta V_{\mathrm{MSP}} = 0$ in this off-resonant condition.

Using the scaling law derived in Ref. [15], we can calculate the resonant $\boldsymbol{M}$ precession cone angle Θ_{res} as

$$\sin^2 \Theta_{\mathrm{res}} = \frac{\Delta V_{\mathrm{MSP}}}{e \nu P R w C g_{\uparrow\downarrow}}, \tag{1}$$

with the elementary charge e; the ellipticity $P = 0.11$, calculated according to Ref. [21]; the resistance $R = 37\ \Omega$ [33] and width $w = 375\ \mu$m of the Co/Pt bilayer;

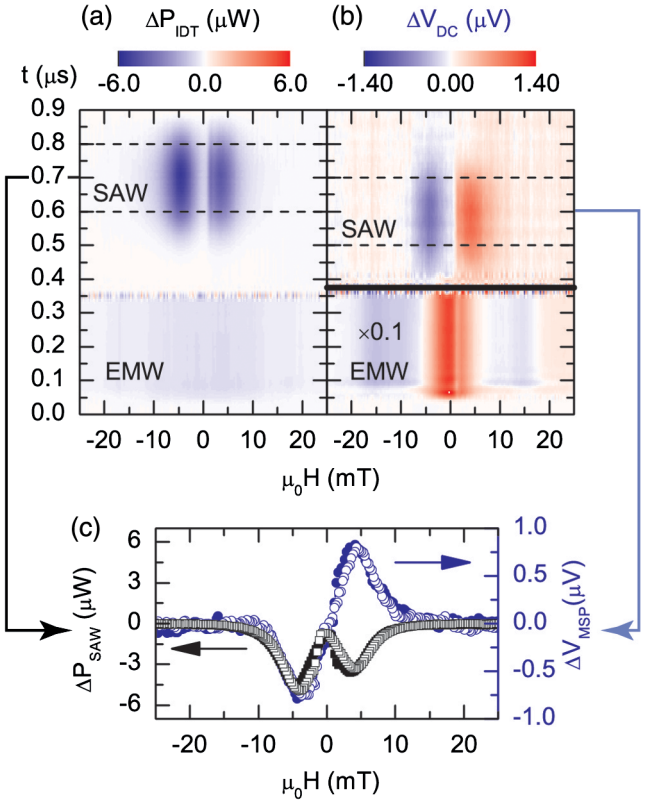

FIG. 4 (color online). (a) ΔP_{IDT} as a function of t and $\mu_0 H$ for $\boldsymbol{H}$ applied at $\alpha = 10°$. (b) $\Delta V_{\mathrm{DC}}(t, \mu_0 H)$ shows EMW rectification (lower part, scaled by 0.1), while the SAW acoustically pumps a spin current which is detected via the inverse spin Hall effect (upper part). (c) We average ΔP_{IDT} and ΔV_{DC} data for the time span indicated by the dashed lines in (a) and (b), respectively. These data correspond to all elastic excitation of FMR (ΔP_{SAW}, left scale) and a spin current (ΔV_{MSP}, right scale).

the constant $C = 4.37 \times 10^{-11}$ m [15]; and the spin mixing conductance of Co/Pt $g_{\uparrow\downarrow} = 6 \times 10^{19}$ m^{-2} [15]. With $\nu = 1.548$ GHz and $\Delta V_{\mathrm{MSP}} = 0.8\,\mu$V from Fig. 4(c), Eq. (1) yields $\Theta_{\mathrm{res}} = 1.6°$, comparing well to values found for photon-driven FMR in Co [15]. Out of resonance, $\Delta V_{\mathrm{MSP}} < 0.1\ \mu$V, and hence the $\boldsymbol{M}$ precession cone angle is $\Theta < 0.6°$, assuming identical P. Using $\Theta_{\mathrm{res}} = 1.6°$, the strain caused by the SAW corresponds to a rf virtual driving field of $\mu_0 h_{\mathrm{ME}} = \frac{1}{2}\mu_0 \Delta H \Theta_{\mathrm{res}} = 73\ \mu$T, with $\mu_0 \Delta H = 5.25$ mT extracted from Fig. 4(c), as the FWHM of ΔV_{MSP} at resonance. Note that this linewidth is just an estimate, since the line shape of acoustic FMR can deviate from a simple Lorentzian due to the particular properties of the magnetoelastic (ME) driving field [24,30]. For acoustically driven FMR, h_{ME} is determined by the magnetic free energy density of the ferromagnetic Co film by [24]

$$\mu_0 h_{\mathrm{ME}} = 2\frac{B_1}{M_s}\varepsilon \cos\varphi_0 \sin\varphi_0, \qquad (2)$$

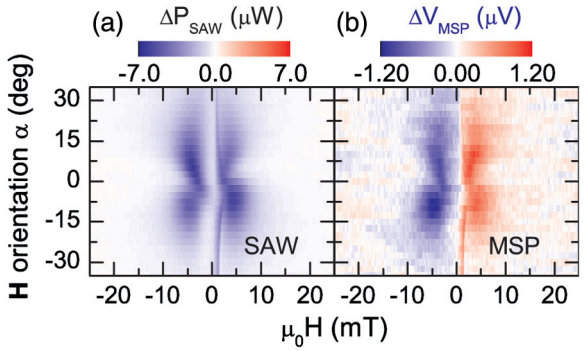

FIG. 5 (color online). (a) ΔP_{SAW} and (b) ΔV_{MSP} as a function of $\boldsymbol{H}$ orientation and magnitude for magnetic field upsweep. The observed angular dependency is characteristic for acoustically driven FMR. The features around 2 mT are due to the $\boldsymbol{M}$ reversal.

where $B_1 = 18$ MJ/m^3 [34] is the magnetoelastic coupling constant of Co, $M_s = 1.17 \times 10^6$ A/m [35] is the saturation magnetization, and $\varphi_0 = 30°$ is the equilibrium orientation of $\boldsymbol{M}$ for $\boldsymbol{H}$ applied at $\alpha = 10°$, calculated using the free energy approach detailed in Ref. [24]. Equation (2) yields a strain $\varepsilon \approx 5.7 \times 10^{-6}$ in the ferromagnet due to the SAW pulse. In an independent experiment, we determined the SAW acoustic power $P_{\mathrm{acoustic}} = 1$ mW by vector network analysis on the input IDT, resulting in a pure strain $\varepsilon = 9.8 \times 10^{-6}$ along $\boldsymbol{x}$ [30]. Thus, according to this order-of-magnitude estimation, the calculated SAW strain is large enough to account for ΔV_{MSP} by elastic spin pumping.

The characteristic fingerprint of acoustically driven FMR is its dependence on the orientation α of the externally applied magnetic field [24]. Therefore, we recorded $\Delta P_{\mathrm{IDT}}(t)$ and $\Delta V_{\mathrm{DC}}(t)$ for $-35° \leq \alpha \leq +35°$ (Fig. 5). Figure 5(a) shows the butterfly angular dependency of ΔP_{SAW} characteristic for acoustically driven FMR. In Fig. 5(b), we observe a finite ΔV_{MSP} only for values of α and H where the acoustically driven FMR condition is met, providing further evidence for phonon-driven spin pumping.

In conclusion, we have shown that a spin current can be generated by microwave phonons via rf magnetoelastic interaction in a Co/Pt thin-film bilayer. By recording both the generated inverse spin Hall voltage proportional to the spin current and the SAW transmission as a function of time for various configurations of the externally applied magnetic field, we are able to discern between effects caused by photonic and phononic excitations. We find that a spin current is generated in the exclusive presence of an acoustic excitation of the Co thin film. This should enable the implementation of, e.g., microelectromechanical systems with the possibility to elastically generate spin current for future spintronic data processing applications. From a fundamental physics point of view, our results are an important step towards the study of the interconversion of phononic and spin degrees of freedom.

Financial support from the DFG, via GO 944/4-1 and SPP 1538, and the German Excellence Initiative, via the Nanosystems Initiative Munich (NIM), is gratefully acknowledged.

*goennenwein@wmi.badw.de

[1] P. Sharma, Science **307**, 531 (2005).
[2] S. Takahashi and S. Maekawa, Sci. Tech. Adv. Mater. **9**, 014105 (2008).
[3] K. Ando *et al.*, J. Appl. Phys. **109**, 103913 (2011).
[4] Y. K. Kato, R. C. Myers, A. C. Gossard, and D. D. Awschalom, Science **306**, 1910 (2004).
[5] V. Sih, W. H. Lau, R. C. Myers, V. R. Horowitz, A. C. Gossard, and D. D. Awschalom, Phys. Rev. Lett. **97**, 096605 (2006).
[6] Y. Kajiwara *et al.*, Nature (London) **464**, 262 (2010).
[7] K. Uchida, S. Takahashi, K. Harii, J. Ieda, W. Koshibae, K. Ando, S. Maekawa, and E. Saitoh, Nature (London) **455**, 778 (2008).
[8] K. Uchida *et al.*, Nature Mater. **9**, 894 (2010).
[9] C. M. Jaworski *et al.*, Nature Mater. **9**, 898 (2010).
[10] C. M. Jaworski, J. Yang, S. Mack, D. D. Awschalom, J. P. Heremans, and R. C. Myers, Phys. Rev. Lett. **106**, 186601 (2011).
[11] R. Urban, G. Woltersdorf, and B. Heinrich, Phys. Rev. Lett. **87**, 217204 (2001).
[12] Y. Tserkovnyak, A. Brataas, and G. E. W. Bauer, Phys. Rev. Lett. **88**, 117601 (2002).
[13] Y. Tserkovnyak, A. Brataas, and G. E. W. Bauer, Phys. Rev. B **66**, 224403 (2002).
[14] M. V. Costache, M. Sladkov, S. M. Watts, C. H. van der Wal, and B. J. van Wees, Phys. Rev. Lett. **97**, 216603 (2006).
[15] F. D. Czeschka *et al.*, Phys. Rev. Lett. **107**, 046601 (2011).
[16] B. Heinrich, C. Burrowes, E. Montoya, B. Kardasz, E. Girt, Y.-Y. Song, Y. Sun, and M. Wu, Phys. Rev. Lett. **107**, 066604 (2011).
[17] In spin Seebeck experiments, the investigation of the phonon-magnon interaction was limited to the application of temperature gradients and thus the nonresonant coupling of phonons and magnons.
[18] K. Uchida, H. Adachi, T. An, T. Ota, M. Toda, B. Hillebrands, S. Maekawa, and E. Saitoh, Nature Mater. **10**, 737 (2011).
[19] H. Y. Inoue, K. Harii, K. Ando, K. Sasage, and E. Saitoh, J. Appl. Phys. **102**, 083915 (2007).
[20] Y. S. Gui, N. Mecking, X. Zhou, G. Williams, and C.-M. Hu, Phys. Rev. Lett. **98**, 107602 (2007).
[21] O. Mosendz, J. E. Pearson, F. Y. Fradin, G. E. W. Bauer, S. D. Bader, and A. Hoffmann, Phys. Rev. Lett. **104**, 046601 (2010).
[22] J. E. Hirsch, Phys. Rev. Lett. **83**, 1834 (1999).
[23] E. Saitoh, M. Ueda, H. Miyajima, and G. Tatara, Appl. Phys. Lett. **88**, 182509 (2006).
[24] M. Weiler, L. Dreher, C. Heeg, H. Huebl, R. Gross, M. S. Brandt, and S. T. B. Goennenwein, Phys. Rev. Lett. **106**, 117601 (2011).
[25] S. Chikazumi, *Physics of Ferromagnetism*, International Series of Monographs on Physics Vol. 94 (Oxford Science Publications, New York, 1997), 2nd ed.
[26] S. Datta, *Surface Acoustic Wave Devices* (Prentice-Hall, Englewood Cliffs, NJ, 1986).
[27] The SAW is a Rayleigh wave and thus has a finite transversal (shear) strain component, as well. We neglect this component for simplicity.
[28] A. Yamaguchi, H. Miyajima, T. Ono, Y. Suzuki, S. Yuasa, A. Tulapurkar, and Y. Nakatani, Appl. Phys. Lett. **90**, 182507 (2007).
[29] L. H. Bai, Y. S. Gui, A. Wirthmann, E. Recksiedler, N. Mecking, C.-M. Hu, Z. H. Chen, and S. C. Shen, Appl. Phys. Lett. **92**, 032504 (2008).
[30] See Supplemental Material at http://link.aps.org/supplemental/10.1103/PhysRevLett.108.176601 for details on possible SAW E field rectification effects and SAW amplitude.
[31] X. F. Zhu, M. Harder, J. Tayler, A. Wirthmann, B. Zhang, W. Lu, Y. S. Gui, and C.-M. Hu, Phys. Rev. B **83**, 140402 (2011).
[32] L. Liu, T. Moriyama, D. C. Ralph, and R. A. Buhrman, Phys. Rev. Lett. **106**, 036601 (2011).
[33] R was determined by a two-point measurement and takes into account that only a fraction of the Co/Pt thin-film bilayer is perturbed by the SAW.
[34] T. Gutjahr-Löser, D. Sander, and J. Kirschner, J. Magn. Magn. Mater. **220**, 1 (2000).
[35] M. Nishikawa, E. Kita, T. Erata, and A. Tasaki, J. Magn. Magn. Mater. **126**, 303 (1993).